Testing and evaluation of reinforced concrete beam-column-slab joint

Authors:

Saddam M. Ahmed, MSc. CE
Anna University
Ph.D. Research Scholar
Faculty of Civil Engineering
Chennai, India

Mosul University
Faculty of Civil Engineering
Mosul, Iraq
civilsaddam@gmail.com

Assoc.Prof. Umarani Gunasekaran, PhD. CE
Anna University
Faculty of Civil Engineering
Chennai, India
umarani@annauniv.edu

Professional paper

Saddam M. Ahmed, Umarani Gunasekaran

Testing and evaluation of reinforced concrete beam-column-slab joint

An experimental investigation of seismic behaviour of identical beam-column subassemblies was conducted by testing two half-scale joint models: one without a slab and the other with a slab. A qualitative model simulating participation of the floor slab was developed by establishing the slab crack patterns (yield lines) and the state of strain in slab bars. Based on the verification results, it was concluded that the joint model improves prediction of seismic behaviour, and that this model allows explicit evaluation of the slab effect on the joint.

Key words:
beam-column joint, modelling, slab effects, beam relaxation, joint shear, cyclic loading

Stručni rad

Saddam M. Ahmed, Umarani Gunasekaran

Ispitivanje i ocjena armiranobetonskog spoja grede, stupa i ploče

Eksperimentalno istraživanje seizmičkog ponašanja identičnih podsklopova greda-stup obavljeno je ispitivanjem dvaju modela spoja u mjerilu 1:2, pri čemu jedan model ima ploču, a drugi nema. Kvalitativni model kojim se simulira sudjelovanje međukatne ploče razvijen je uspostavljanjem obrazaca pojave pukotina u ploči (linija popuštanja) i stanja deformacije u armaturi ploče. Na bazi kontrolnih rezultata zaključeno je da model spoja dovodi do boljeg predviđanja seizmičkog ponašanja te da taj model omogućava eksplicitno ocjenjivanje djelovanja ploče na spoj.

Ključne riječi:
spoj grede i stupa, modeliranje, utjecaji ploče, rasterećenje grede, posmik spoja, cikličko opterećenje

Fachbericht

Saddam M. Ahmed, Umarani Gunasekaran

Prüfung und Bewertung der Stahlbetonverbindung von Balken, Stütze und Deckplatte

Experimentelle Untersuchungen des seismischen Verhaltens aus Balken und Stütze bestehender Einheiten wurden durch Versuche an zwei identischen, im Maßstab 1:2 angelegten Modellen der Verbindungen durchgeführt, zum einen mit, zum anderen ohne Betondeckplatte. Ein qualitatives Model, das die Mitwirkung der Deckplatte simuliert, ist durch die Auswertung der Rissbildung im Beton und des Spannungszustandes im Bewehrungsstahl entwickelt worden. Aus den Prüfungsergebnissen folgend, verbessert das Modell der Verbindung die Vorhersage des seismischen Verhaltens und ermöglicht die explizite Ermittlung des Einflusses der Deckplatte.

Schlüsselwörter:
Verbindung von Balken und Stütze, Modellierung, Deckeneinfluss, Balkenentlastung, Schublast in Verbindungen, zyklische Lasten

1. Introduction

During strong earthquakes, the performance of multi-storey RC frame buildings mainly depends on the behaviour of beam-to-column joint subassemblies. Recognizing the importance of understanding the behaviour of subassemblies, many experimental studies have been carried out focusing on the behaviour of external [1] or internal [2-4] beam-to-column connections under cyclic loading. In most of the previous studies, the test subassemblies usually consisted of connections with main beams without a slab. In a real structure, however, the slab is normally cast monolithically with the floor beams and interacts structurally with the members framing into a joint. Several series of tests were conducted on reinforced concrete slab-beam-column subassemblages in which the participation of the slab in resisting the lateral load was investigated. The tests were conducted on both small and large scale models with different geometries, boundary conditions, material properties, beam and column reinforcement layouts, and loading histories [5-9]. Most of these research studies focused on investigating how much a floor slab contributed in increasing the beam flexural strength thereby, reducing the column-to-beam moment strength ratio, (when the slab was in the tension zone of the beam section). It has been suggested that, to ensure a satisfactory performance of connections, a certain minimum width of the floor slab must be considered effective in designing beam-to-column connections. These tests had a major impact on the design codes. Therefore, different code provisions were recommended to consider the "Tension flange of a slab" at the beam column subassemblies, e.g. ACI 352R [10], NZS 3101 [11] and CSA-A23.3 [12]. However, limited research was concerned with the effect of floor slabs on joint shear behaviour, although some researchers did indicate that floor slabs could impose additional shear demands on joints [9].

Zerbe and Durrani [13, 14] conducted several experimental studies on beam-column joints (interior and exterior) including slabs, and transverse beams on a subassembly. The authors paid attention to study the influence of slabs in increasing the frame strength. These tests demonstrated clearly that "beam growth" phenomenon occurs and that it causes an increase in column moments and shear forces. This phenomenon ("beam elongation") was first described by Fenwick and Fong [15]; and it has a remarkable influence on the strength and overall stability of reinforced concrete (RC) framed structures. Recently, it was very clearly seen in the 2010-2011 Canterbury earthquakes [16].

Based on experimental investigations, many analytical studies have been carried out to investigate the effect of different parameters on the seismic behaviour of the connection region and predict the load–deformation responses. Youssef and Ghobarah [17] modelled the joint (Figure 1.a) with two diagonal translational springs connecting the four opposite corners of the panel zone to simulate the joint shear deformation. At the beam/column interface, 12 springs were provided to simulate all other modes of inelastic behaviour. Elastic element members were used for the joining elements. This model requires a separate constitutive model for each spring. The model was verified with a set of comparisons with experimental measurements.

Lowes and Altoontash [18] developed a joint element (Figure 1.b) that represents the nonlinear behaviour of the joint by developing constitutive relationships of material, geometric and design parameters and implementing it to the joint element. The joint element has four exterior nodes each with 3DOF, thus the joint is compatible with traditional 2D beam-column elements. The cyclic response parameters were calibrated based on experimental data. Subsequently, Mitra and Lowes [19] improved this model by modifying the element definition. A compression-strut model was used to simulate the joint strength losses. Kim and LaFave [20] used a statistical approach to evaluate the effect of some key parameters such as panel geometry, concrete compressive strength, confinement due to joint reinforcement, column axial load, and bond characteristics of the longitudinal reinforcement to the joint behaviour. It was concluded that the shear capacity of the panel joint mainly depends on concrete compressive strength. However, joint panel geometry has only a slight effect on the seismic performance. After determining the most influential parameters to the joint shear stress–strain behaviour, they proposed an equation representing the joint shear strength.

Further studies were based on refined nonlinear finite element models to accurately capture the behaviour of interior joints and derive useful conclusions from numerical-experimental comparisons [21, 22]. However these approaches needed higher computation time, accurate meshing, sufficient storage for the results, and most of all these methods were limited to single connections.

In general, all these methods did not account for the beam elongation or slab effects at the connections. Fenwick and Davidson [23] proposed a simple analytical model for beam elongation without considering for the slab effect, as shown in Figure 1.c. At the end of each beam, a composite element was placed that consisted of one steel element and one concrete element on the top and bottom of the section. A six storey, three-bay frame was analyzed, with and without the beam elongation elements. Obvious changes in the distribution of forces between the beam and columns were observed. Greater beam elongation occurred with greater beam depths and storey drift ratios. So it was suggested that the beam elongation is proportional to the beam depth and number of bays.

Models developed by others including slab effect and beam elongation, such as Shahrooz et al [24]. The study was limited to the monolithic loading only, or did not simulate the subassembly hysteresis loop pinching and stiffness
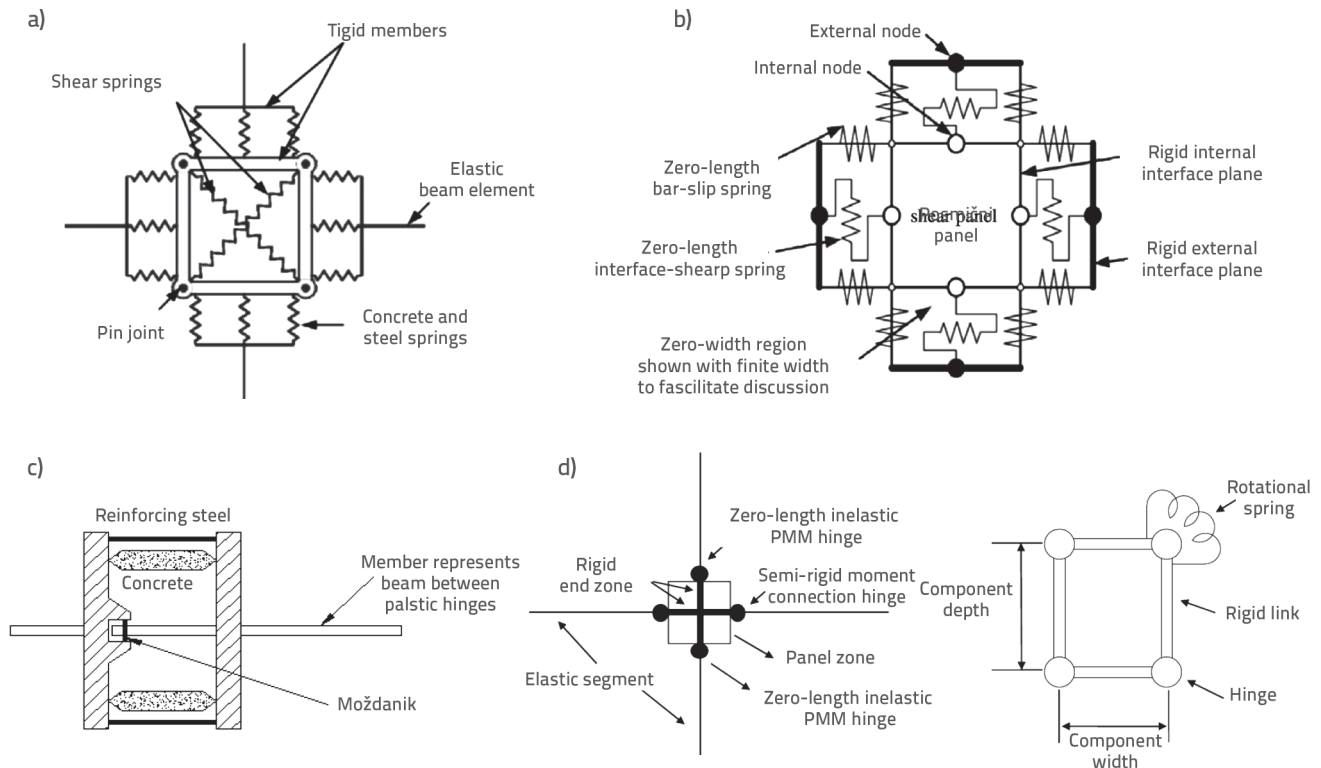
a)

b)

c)

d)

Figure 1. Multiple spring joint models by various researchers: a) Youssef and Ghobarah joint model [17]; b) Lowes and Altoontash joint model [18]; c) Beam elongation model [23]; d) Unal and Burak joint model [28]

degradation [25], but the increase in strength due to slab was achieved. Other very sophisticated models considering both effects were developed by Lau [26] and Peng [27], a floor model was used to simulate the response of a linking slab. The linking slab was modelled using a series of struts, connected both in parallel and in series, to simulate the horizontal shear transfer in the plane of the floor slab as well as out-of plane bending of the floor slab. As the model is very sophisticated, it requires large computational effort. It should also be noted that despite the relative complexity of the model, there were some discrepancies between the analytical predictions and the experimental results. The errors were mainly due to elongation of plastic hinges not being captured accurately; however, its applicability in indeterminate structures or structures under cyclic loading is uncertain.

More recently, Unal and Burak [28] developed an analytical model to represent the cyclic inelastic response of reinforced concrete joints. The model considered the panel joint as a rigid zone and all the effects of shear distortions observed in these regions were assumed to be lumped at the rotational springs located at the four corners of the joint and between the rigid links as shown in Figure 1.d. To evaluate the properties of these rotational springs a parametric model that predicts the joint shear strength versus strain relationship was developed by investigating several previous experimental studies on RC beam-to-column connection subassemblies subjected to cyclic loading hence establishing an extensive database.

In order to take the presence of the slab into account, the effective beam width defined in ACI 318 [31] was considered and the reinforcement placed in the flange was included implicitly as a factor of slab index "SI". The nominal moment strength for the flanged section is calculated and divided by that of the rectangular beam section having the same depth and web width:

$$\text{Slab Index (SI)} = \frac{M_n(\text{Flanged section})}{M_n(\text{Rectangular section})} \qquad (1)$$

It is observed that, in general, the seismic behaviour of beam-to-column connection subassemblies is reasonably predicted not only for the overall lateral load–storey drift response, but also for the element responses.

It can be seen from the above discussion, that while the beam elongation and slab effects are seldom considered in frame analysis, they may be significantly affecting the frame lateral strength and the demands on the columns.

However existing models either do not have a realistic loop, or are too complex. To this purpose, the present paper initially analyses some test results, relevant to two subassemblies' specimens tested under cyclic loads, to evaluate the effect of the floor slab on the beam strength, column strength and panel joint shear demands. Successively, numerical simulations based on Finite Elements Models (FEMs) developed using the RUAUMOKO-2D [29] have been performed to apply a simple model for a beam-column subassembly with a reasonable

calibration for both the beam elongation/relaxation and the slab effects. The model developed should be capable of simulating pinching effect and stiffness degradation with expected hysteretic loop as in reinforced concrete structures; and finally, it should validate the proposed computational method with the previous and existing test results.

2. Experimental program

2.1. Design of prototype frame

The prototype building was 27.6 m long, 20 m wide, five-storey high and four perimeter frames, spanning four bays in the longitudinal direction. The framing systems in the transverse direction were not considered in this study. The elevation view of the perimeter frame is given in Figure 2.a. Each bay spanned 6.9 m, and the storey height was 3.5 m throughout the building. The typical lower interior subassembly, illustrated in Figure 2.b, was considered for the experimental investigations. The prototype structure was designed for zones of high seismicity,

Seismic Zone IV, in accordance to the UBC [30] assuming standard occupancy, type D-stiff, soil profiles. The effective seismic mass at each floor was assumed to be 590 t (1,300 kips).
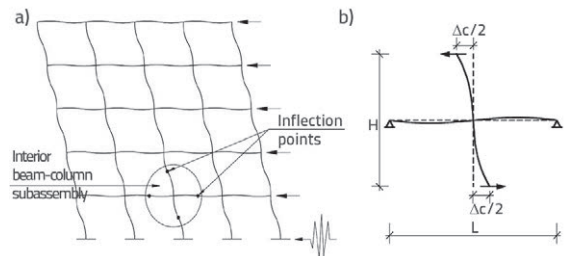
Figure 2. a) Prototype frame subjected to seismic lateral loading; b) Modelling the interior beam-column subassembly

The same size members were used over the frame height. All the beams and columns were designed in such a way, that all yielding would occur only in the beams (satisfying the strong-column weak-beam concept), and satisfied most of the ACI-
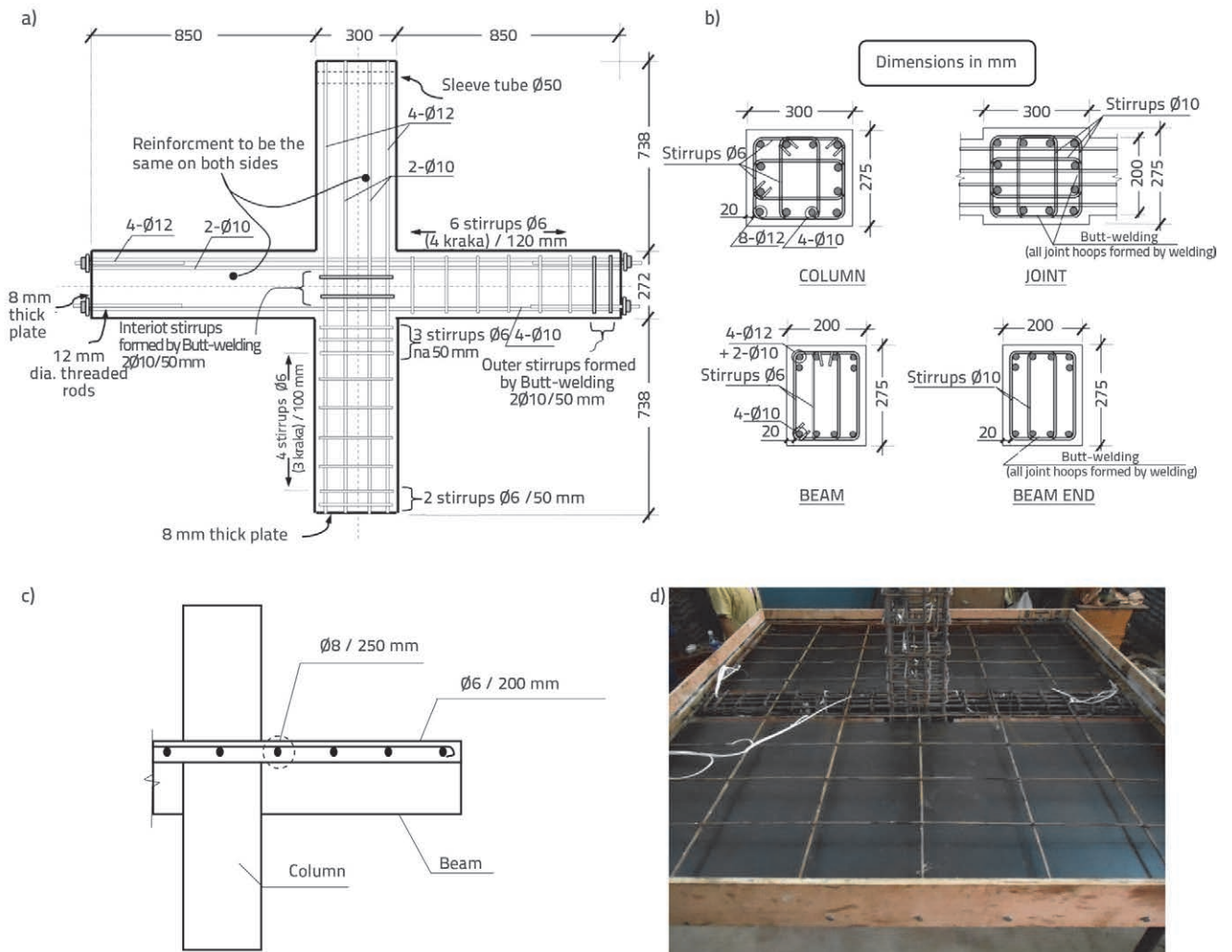
Figure 3. Reinforcement details of the specimens: a) Longitudinal reinforcement details (specimens J, JS); b) Section details (specimens J, JS); c) Section in the slab (specimen JS); d) Reinforcing view (specimen JS)

318 [31] recommendations. The static pushover analysis, with inverse triangular lateral loads, was performed to identify the frame demand (the frame reached the design drift at the UBC design force). The design storey drift was assumed to be 2 % as per UBC (Section 1630.10 [30]) and the corresponding base shear was 2,000 kN.

2.2. Test specimens

The two specimens represent approximately half-scale models. Each specimen consisted of a column, two beams framing into the column on opposite sides, without transverse beams. The specimens had 275×300 mm columns cross section and 275 mm deep × 200 mm wide beams. The geometry and reinforcement details of the test specimens are shown in Figure 3. The two specimens had the same size and reinforcement detailing for the beams, columns and beam-column joint but the first subassembly labeled "J" was constructed without a floor slab, while the second subassembly labeled "JS" had a slab, cast monolithically with the beam. The overall floor slab dimensions were 2.0 m × 2.0 m, with an average thickness of 63 mm. The reinforcements of the slab were Ø6/250 mm in the parallel direction of the beam (longitudinal direction), and Ø8/250 mm in the transverse direction. For each subassembly, all members were cast at one time (Figure 4).

Figure 4. Construction of test specimens: a) Casting of the test specimen JS; b) Curing of the test specimens

Concrete was prepared according to ACI 301 [32]. The concrete consisted of crushed stone processed from natural rock in accordance with ASTM C33 [33] specifications. An aggregate maximum size of 10 mm and a slump of 120 mm were used to accommodate any steel congestion in the joint region and the minimum clear cover of 20 mm.

Wet coverings saturated with water were used after the concrete had hardened enough for curing the specimens and the control specimens as shown in Figure 4.b. The often specified 14-day curing commonly corresponds to approximately 70 % of the specified compressive strengths according to ACI 301.
Before the execution of the tests on the joint specimens, the mechanical properties of the constituent materials, namely concrete and steel, were determined. Eight concrete control specimens were prepared during each specimen casting for this purpose. Testing of the control samples was conducted following the guidelines of the testing requirements in ASTM C39 [34]. Table 1 summarizes the actual compressive strengths of the concrete at 28 days and on the testing day. These values provided practically identical values in terms of mean strength. With respect to steel, 12 bars having 6, 8, 10 and 12 mm diameters were subjected to tensile tests thus determining the mean yielding strength f_y, yielding strain ε_y, ultimate tensile strength f_u, and ultimate elongation ε_u. The values are given in Table 2.

Table 1. Concrete compressive strength, f_c'

Compressive strength [MPa]	Test specimens		
		J	JS
28-days		44,89	37,06
At testing day		50,55	44,83

2.3. Test set-up and loading protocol

The tests were carried out by applying the vertical displacements at the ends of the beams, as shown in Figure 5. The column was linked to a universal hinge connector at the bottom and to a box frame (with a swivel connector) at the top. The end of each edge-beam was linked to the 250 kN hydraulic actuator by a pinned-axial end. Thus the two ends of the beams and the top and bottom of the column were all pin-connected in the loading plane, to simulate inflection points of a frame structure subjected to lateral earthquake loading. The column pin-to-pin storey height (H) was 1.70 m, and the beam pin-to-pin span length (L) was 2.2 m. The edges of the floor slab were left free to negate any possible effect of slab membrane action that might have provided additional confinement to the joint region. A box frame was installed on the top of the column in order to guide

Table 2. Reinforcement properties

Ø [mm]	A_{sb} [mm²]	Yield strength, f_y [MPa]	Yield strain, ε_y [µmm/mm]	Ultimate strength, f_u [MPa]	Elongation [%]
6	34,9	469,3	2420	604,3	23,0
8	52,6	459,0	2300	578,4	18,0
10	79,2	451,1	2375	539,1	19,1
12	112,3	477,2	2330	603,2	10,9

specimen rotations along the longitudinal direction only. Uni-axial shear was statically applied at the ends of the beams by hydraulic actuators.
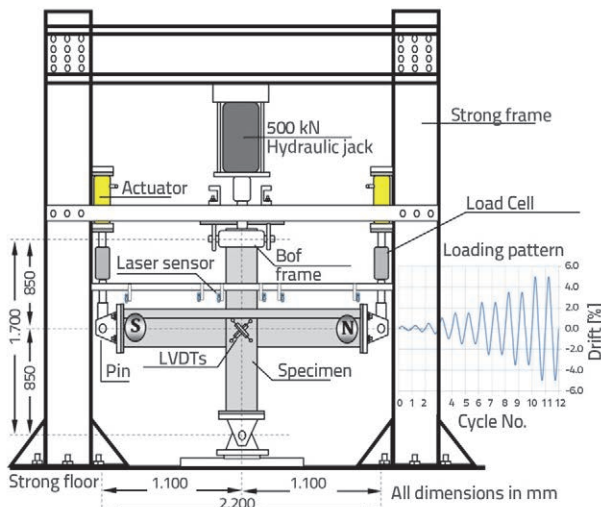

Figure 5. Test set-up and loading pattern

The pattern of cyclic displacements applied by the actuator during each test is given in Figure 5. The displacement at the ends of the beams was increased by steps from 0.25 % up to a drift of 1.0 % with one cycle for each drift amplitude, then two cycles for each drift amplitude greater than 1 %. A total of twelve displacement cycles were applied up to 5 % drift cycle. The choice of different drift amplitudes was related to the expected cracking and yielding drift values, which are in the range 1.0-2.0 %. Thus, it was possible to better monitor the cracking and yielding phenomena which occurred during the initial part of the tests.

The axial force was applied by a standard hydraulic jack to a steel cap provided at the top end of the column. The vertical load was kept constant throughout the entire test, (A constant axial nominal compression load of 10 % of the column axial capacity was applied) to provide the necessary column confinement to the connection.

Instrumentation used in each specimen was as follows; six laser sensors, with a reading error of less than 8 μm fixed above the beam were used to measure the beam response. Electrical resistance strain gauges mounted on reinforcing bars at key positions in and around the connection. The deformations of the joint panel were detected through linear variable differential transducers (LVDTs) installed in an "×" shape on the face of the joint. Load cells were installed between the actuators and the beams to measure applied forces. Hydraulic actuators were used having maximum force capacity of +250/-100 kN and a stroke of ±100 mm. A data acquisition system (DEWE-43) was used to monitor and control the displacement and force feedback signals. The rate of sampling was 100 points per second (100 Hz).

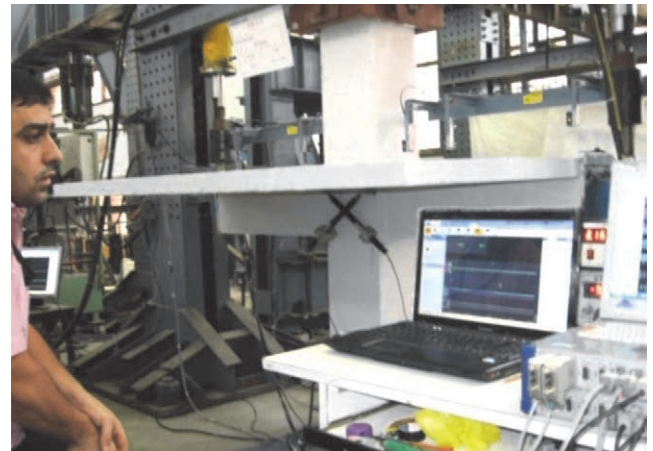Instrumentation used as shown in Figure 6, where the test apparatus is displayed.

Figure 6. View of a test in progress

3. Experimental results

3.1. Test observations

The two specimens performed in a ductile manner, and explicitly showed a strong column-weak beam behaviour which is essentially required by the code provisions for the ductility frame. The plastic hinges were noticed at the beam/column interfaces and had only fine cracks in the column over the whole height, indicating that the column did not suffer major inelasticity.

At the panel zone (beam-column intersection zone) minor cracks were observed at drift ratios of 1.5 %. Then the width of these cracks gradually increased to form diagonal cracks on both joint faces. A comparison of cracks in specimen J with specimen JS showed remarkable differences, indicating the influence of the floor slab on the failure mechanism. The panel zone in specimen J was observed resulting in a lower deformation capacity behaviour and the width of the cracks were recorded less than 0.2 mm. Large crack widths were observed in specimen JS. These joint cracks were propagated to the slab and its width significantly increased at the slab/column intersection resulting from lower deformation capacity for the joint compared to the slab, indicating that this portion of joint was exposed to a large stresses. In general, the joint cracks opened and closed on load reversal. The concrete cover remained intact until the end of the test. Figure 7 shows the joint cracks observed at the end of the test in the two specimens. Even at high drift levels the joint in both specimens exhibited good behaviour with almost no spalling of concrete in or near the joint region.

In the beam plastic hinge region, the yield points of the specimens are determined from the load–displacement curves, and verified by examining the yielding of individual bars in the beam.
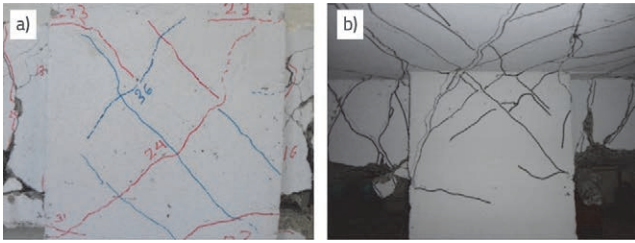
Figure 7. Joint cracks at the end of the test for the test specimens J and JS

The first yielding on the bottom beam bars occurred during 1.5 % drift cycles, and most of the beam bars yielded during 3.5 % drift cycles. The beam bar yielding spread to a length equal to the effective beam depth from the column face during the 3.5 % drift cycle, meaning that beam hinging developed adjacent to the beam/column interfaces. Concrete crushing and spalling were noticed at the bottom of the beams beside the column during the 5 % drift cycle. The 4-Ø10 bars in the bottom of the north beam were exposed first, and then in the south beam, for both the specimens. The overall plastic hinges developed at beam/column interfaces at the end of the test are shown in Figure 8.
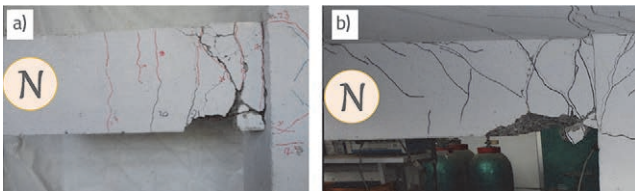
Figure 8. Final damage state at the north beam of specimens J and JS

During testing, the cracks in the slab were observed to open and close at drift ratios of up to 1.5 % for specimen JS. Beyond this stage, the slab started to yield, and approximately 45° cracks were observed at 2.5 % drift cycle. The width of these cracks

gradually increased until the tests ended. Slightly larger cracks (2.6 mm) occurred transversely in the slab. In general, these cracks were found to be symmetric in shape and width in the N–S and E–W directions. The overall crack patterns observed in the slab of the specimen JS, are shown in Figure 9.

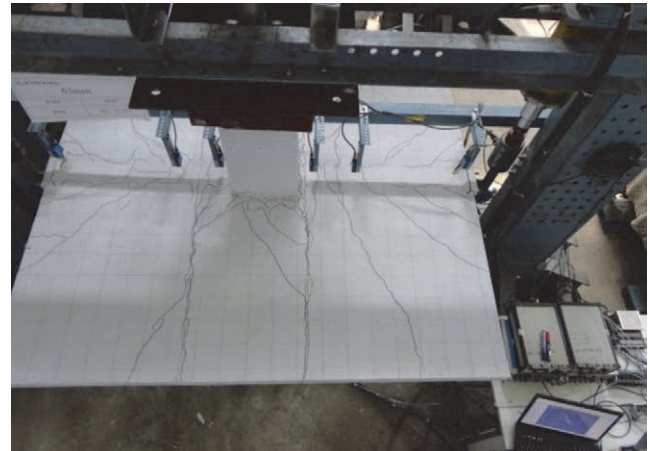
Figure 9. Crack patterns in the slab of specimen JS

3.2. Load–displacement response

The beam rotation was calculated from the relative laser sensor displacement readings at the beam end and near the column face. The hysteretic curves of the moment against beam rotation (north beam) for the two specimens are presented in Figure 10.a. They were typical in that they exhibited less pinching effect, and also they showed similar performance in stiffness and strength degradation during repeated drift cycles of the same magnitude. These were attributed to no bond slip through the joint region. It is clearly seen that the longitudinal slab steel participates in the flexural resistance especially in the negative direction of
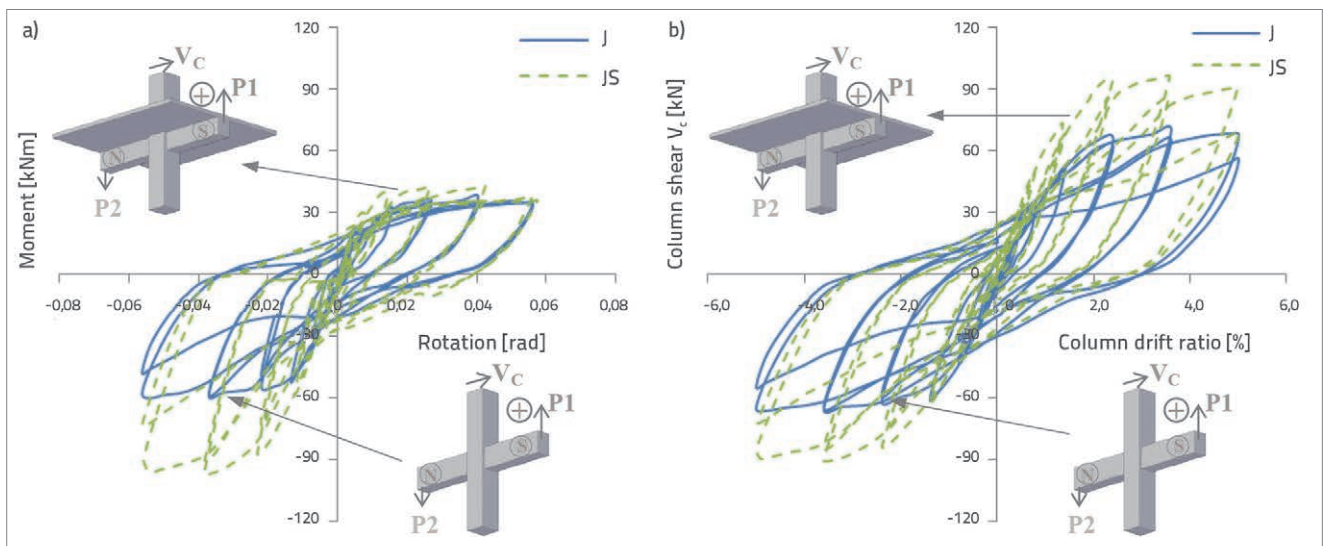

Figure 10. Hysteretic curves of: a) North beam moment vs rotation; b) Column shear vs drift ratio

loading (slab reinforcement in tension). The presence of the floor slab increases the beam resistance capacity in tension and compression as confirmed from Figure 10.a, thereby demanding additional column strength in both directions of loading. This concept is proven by the column shear-drift results shown in Figure 10.b.

The envelope curves of the north beam moment vs. rotation for the two specimens are shown in Figure 11.a. At the early stage of the testing (up to drift cycle of 1 %) the two specimens showed approximately similar beam strength. During large drift levels of above 1 %, the rate of increase in beam strength became significantly higher for the specimen JS compared to the specimen J.

Specimen JS exhibited the largest beam moments in both directions of loading as compared to specimen J. The average values of the increased beam flexural strength for the two specimens at all loading steps were calculated and a comparison of these values of specimen with slab (JS) and without slab (J) were made. It was found that the increases in the beam strength in the negative direction of loading (slab in tension) was 67.1 % for specimen JS compared to specimen J, while these increases in the positive direction (slab in compression) of loading was 16.7 % for specimen JS compared to the specimen with no slab. Figure 11.b compares the envelope curves of the column shear vs. the drift ratio for the test specimens. Similarly a comparison for the increases in the storey shear resistance was made and it was found that the slab increased the storey shear resistance by 33 % for specimen JS relative to the specimen without slab.

3.3. Slab bar strains

The test specimen JS had five longitudinal slab bars (Ø6 mm). Each longitudinal slab bar was instrumented with a strain gauge located crossing the centreline column. Figure 12 illustrates the strain profiles of longitudinal slab bars at peak drift points

of various cycles. Before yielding, as the drift increased all longitudinal slab bars experienced a continuous increase in the strain. Therefore it is clear that the effect of slab participation to beam moment strengths and joint shear demands increase with the increase of the drift levels. The slab bar nearest to the edge-beams underwent the fastest strain increase. Onset of slab bar yielding occurred during the 2.5 % drift cycle and most of longitudinal slab bars yielded by 3.5 % drift.
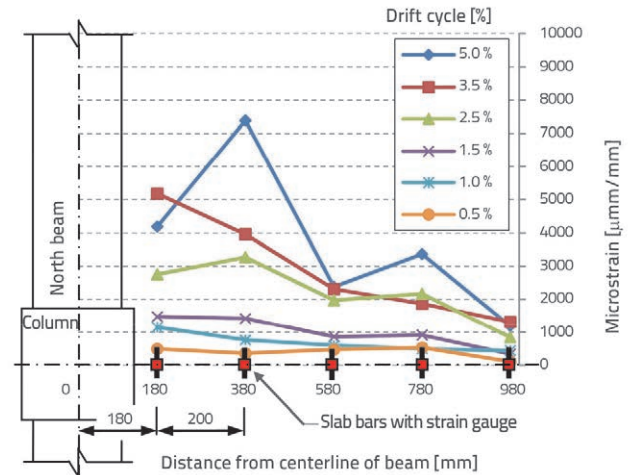

Figure 12. Slab bar strain profiles vs drift cycle (%) for the specimen JS

3.4. Determinations of joint shear stress and strain

In the beam-to-column moment connection, the compression or tension interior couple forces from the beam produce a large shear in the panel joint. If the joint is unable to resist such shear, yielding will occur in the panel region. To monitor the overall joint shear deformation in an average sense, two LVDTs were installed at the face of the joint in each specimen in an "×" shape. Considering the two triangles formed by the LVDTs, the angular changes as shown in Figure 6 were
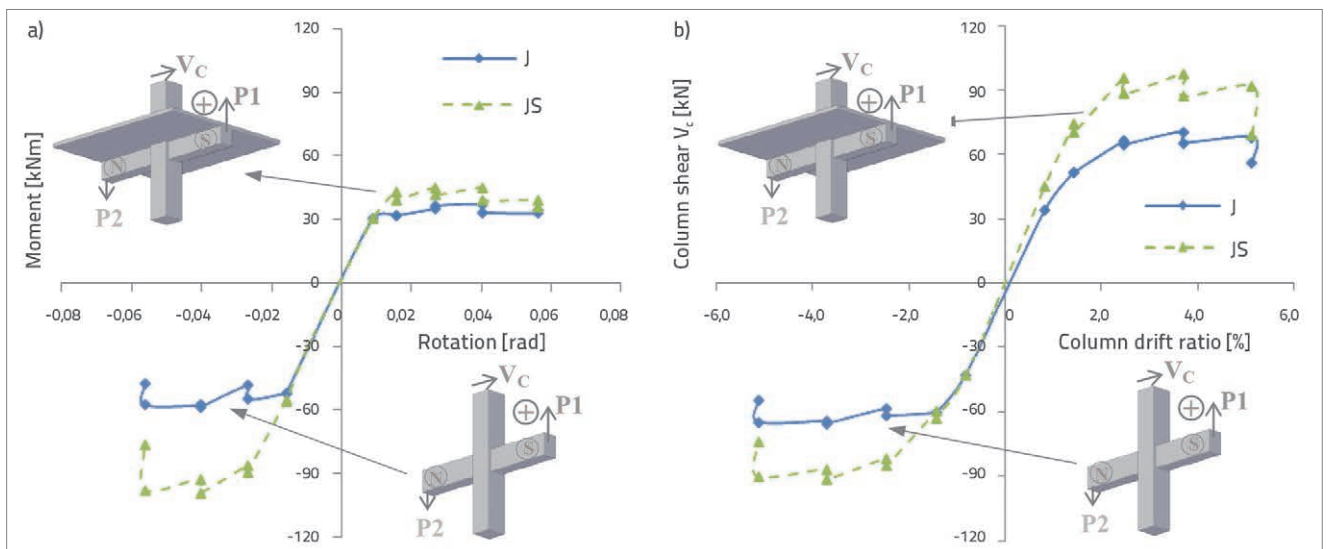

Figure 11. Envelope curves of: a) North beam; b) Column

measured for each step. Then, the joint shear deformation was computed as an average of the two angular changes at the face of the panel. In this study, the joint shear strain was calculated using Equation (2):

$$\phi_j = \frac{\sqrt{b^2 + h^2}}{2 \cdot b \cdot h} [\Delta_1 + \Delta_2] \qquad (2)$$

where ϕ_j (radian) represents the joint shear deformations, b and h are the width and height of the panel zone area between the two LVDT anchor points respectively. While, Δ_1 and Δ_2 are the displacements measured using LVDTs positioned diagonally over the panel. On the other hand the joint shear strength is evaluated, by studying the equilibrium of the horizontal forces on a horizontal plane at the mid height of the joint, as shown in Figure 13.
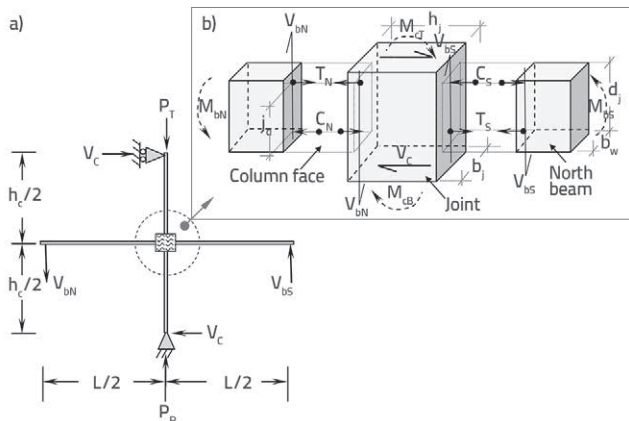

Figure 13. Free body diagrams of: a) a typical interior subassembly test setup; b) its joint panel

The joint shear force can be represented through tension and compression couples at the joint face, as the tension forces acting on the south and north faces of the panel respectively.

Thus, the effective horizontal shear force acting on the joint panel, V_{jh} can be calculated as:

$$V_{jh} = (T_N + C_S) - V_c \qquad (3)$$

where V_c is the column shear force, which can be estimated by the equilibrium of forces at the beam-end actuator forces as:

$$V_c(h_c) = V_{bN}\left[\frac{L}{2}\right] + V_{bS}\left[\frac{L}{2}\right] \qquad (4)$$

While, the tension components of the equivalent couples on the north and south beam can be expressed as:

$$T_N = \frac{M_{bN}}{j_d}; \quad C_S = \frac{M_{bS}}{j_d} \qquad (5)$$

where M_{bN} and M_{bS} are the beam moments at the joint in the north and south face respectively; j_d is the beam internal moment arm at the north and south beam/column interfaces ($j_d = h_b - d' - d''$), which were assumed to be 195 mm; then, the joint shear can be expressed as follows:

$$V_{jh} = \left[\left(\frac{M_{bN}}{j_d}\right) + \left(\frac{M_{bS}}{j_d}\right)\right] - \left[V_{bN} + V_{bS}\right]\left(\frac{L}{2 \cdot h_c}\right) \qquad (6)$$

Since M_{bN}, M_{bS} are the beam moments at the joint face which are equal to $V_{bN} \times (L/2 - h_j/2)$, and $V_{bS} \times (L/2 - h_j/2)$, respectively, by substituting these into Equation (6), the joint shear can be rewritten as:

$$V_{jh} = \left[V_{bN} + V_{bS}\right]\left(\frac{L - h_j}{2 \cdot j_d} - \frac{L}{2 \cdot h_c}\right) \qquad (7)$$

where L is the total length of the beam (includes south and north beam), h_j is the depth of the joint panel (depth of the column), and h_c is the total height of the column; (subscripts S and N refer to south and north, respectively). Then, the joint shear stress, τ_{jh} can be computed as follows:
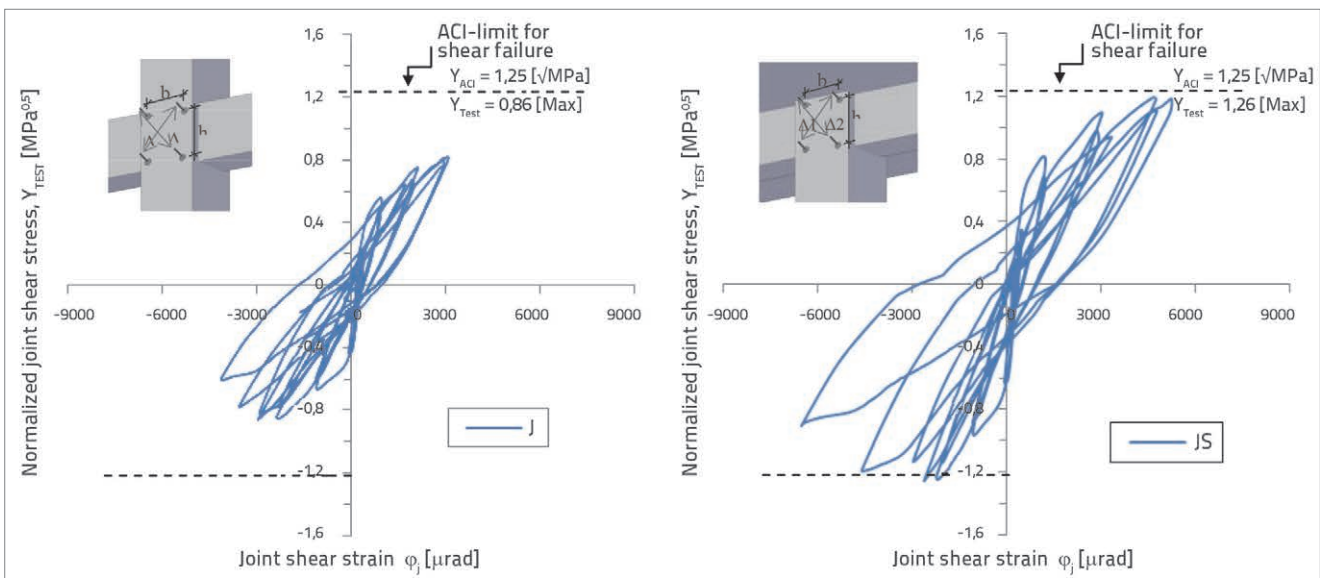

Figure 14. Normalized joint shear stress vs joint shear strain for the joints J and JS

$$T_{jh} = V_{jh}/A_{jh} \qquad (8)$$

where A_{jh} represents the effective cross sectional shear area, which was calculated based on ACI 352R-02 (Section 4.3.1). The joint shear stress can be normalized by $\sqrt{f_c'}$ (square root of concrete compressive strength) as:

$$Y_{Test} = T_{jh} \Big/ \sqrt{f_c'} \qquad (9)$$

Figure 14 shows the normalized joint shear stress γ_{Test} versus joint shear strain for the both specimens. It can be noticed that the joint in specimen with slab exhibited similar joint shear deformations at a relatively slow rate of increase in joint shear deformation during the early stages of the tests. However, the rate of increase became higher during 3.5 % and 5 % drift cycles. Specimen J exhibited smaller joint shear deformation contributions to drift than the specimen JS.

The maximum normalized joint shear γ_{Test} values were close to the shear strength factor of, γ_{ACI} (1.25; seismic joints confined on two opposite vertical faces) recommended by ACI 352R [10] in specimen JS. However, the stresses were below this limit for the case of the beam-column joint without a slab (J). This means that extra compression stress would act on the joint from the bottom fibre of the beam, in addition to an increase in the tension stress from the top fibre of the beam. Thus the floor slab increased significantly shear deformation and stresses of the joint as shown clearly in Figure 14.

3.5. Experimental evaluation for the beam elongation/relaxation

One of the factors that affect the behaviour of subassemblies is related to the expansion of the plastic hinge regions, and the resulting elongation of the beams. In this investigation, the elongation of the main beams on the behaviour of connections was insignificant at a small drift level below 1.5 % (less than 1.5
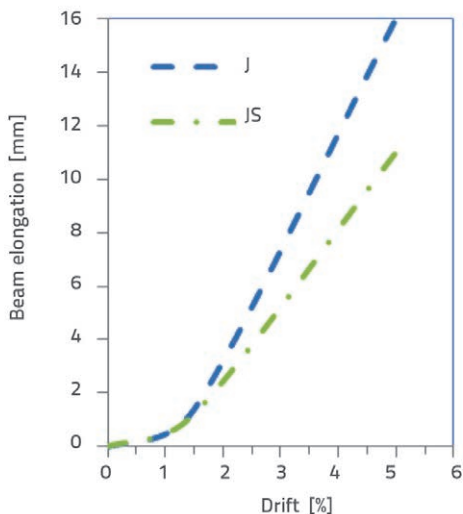

Figure 15. Beam elongation/relaxation

mm for both specimens). Beyond this stage, the beams elongation was significantly increased due to extensive flexural cracks developed in the beams on either face of the column, as shown in Figure 15. The beam elongation exhibited by these specimens was similar to or larger than those found in the literature [14]. However, the effect of the restraint by a floor slab to the elongation of main beams is obvious from their smaller growth.

4. Development of an analytical model

The developed model shown in Figure 16 was used to simulate the beam–column joint region. A similar model had originally been used to represent the gap opening and beam elongation behaviour at the beam–column joints, without considering for the floor slab effect in reinforced concrete frame and precast systems, Kim et al [35], and it was modified for use in the current study. The model was constructed in RUAUMOKO-2D [29] and it uses elements from the standard library.
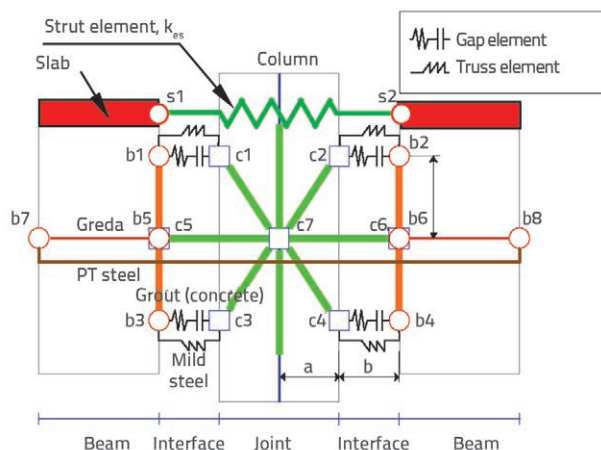

Figure 16. Development of the joint model

Nodes c1 to c7 and b1 to b8 are associated with the column and beam, respectively. In the column, Nodes c1 to c6 are slaved to a master node (Node c7), so that all the seven move together as a rigid body. Beam Nodes b2 and b4 are slaved to b6 in the same way. Nodes s1 and s2 at the top face of the beam are introduced to connect the slab element. Joint deformations are not modeled. Moments are transferred between the beam and column by horizontal tension and compression compounds between node pairs, e.g. b2–c2. Two parallel sets of elements connect the nodes in each pair. One is an inelastic truss element that simulates the reinforcement and resists axial tension or compression forces. The other is a gap element which has inelastic properties in compression without tension strength, thereby simulating the behaviour of cracked concrete and the beam elongation that associates cracking. The figure shows only two nodal pairs on either side of the column, the model uses ten gap elements, equally spaced, in order to replicate the gradual lift-off that occurs in practice. Shear is transferred across the interface by

providing very stiff vertical springs at Nodes b5–c5 and b6–c6. A pre-stressing element (PT steel) was used only for the post-tensioned precast member simulation, but not for the reinforced concrete system.

Models excluding and including slab effect were verified with the previous and existing test data. The element properties were directly related to the physical properties for each component. The beams and columns are modelled using 4-noded frame elements [29] with cracked sectional properties ($I_e = 0.4 I_g$). The truss element for the mild steel with Clough degradation hysteresis [36], as shown in Figure 17, was selected to provide the appropriate force–displacement characteristics. The strain-hardening ratio of the steel was 0.02. The stiffness property of mild steel is assigned, based on the yield length which is assumed as the sum of the depth of the beam, plus twice the anchorage length specified in the ACI 318-02 [31]. The properties of the concrete gap elements were selected, based on the length of plastic hinge [37] and an elasto–perfectly plastic stress–strain curve with a yield strain of 0.003 at the compressive strength f_c'.
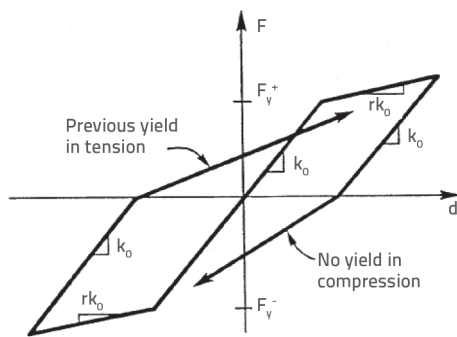

Figure 17. Clough degradation stiffness hysteresis

4.1. Slab modelling

Large tensile strains develop in the reinforcement across the slab near the longitudinal beam, and decrease with increasing distance from the beam. This continuous transition is idealized in Figure 18 by a modified multi flexible springs with rigid links. These rigid links connect the end of the plastic hinge of the beam to the points where the slab longitudinal reinforcement bars enter within the entire effective slab segment.

In the current model, the effective slab segment between the yield lines is where cracking at $45°$ angle is expected. The effective steel is assumed to be anchored outside this zone. The flexible springs between the rigid links reflect the deformability of the floor system (resulting from crack opening) when subjected to in-plane tensile actions.

The stiffness property of slab reinforcing steel, ($k_{bi} = EA/L_s^i$) is calculated, based on the length of yield of each bar within effective width, as follows:

$$L_s^{(i=1)} = (2l_p + d_c) + S \qquad (10)$$

$$L_s^{(i=2, 3, \dots n)} = L_s^{(i=1)} + 2S \cdot (i - 1) \qquad (11)$$

where, l_p is the plastic hinge length, s is the spacing between longitudinal reinforcing bars and d_c is the column width. The slab element stiffness, k_{es} is the sum of the slab bars stiffness's within the effective segment of the tension slab. It is assumed that tensile stress capacity of concrete is zero and truss element for the slab reinforcing steel with Clough degradation hysteresis, was selected.
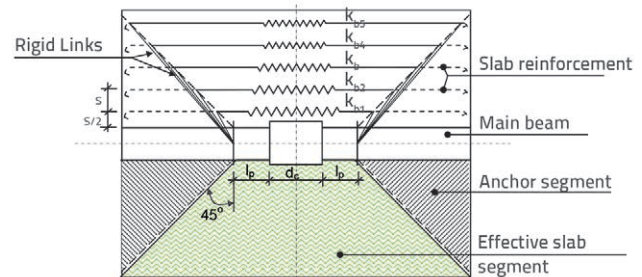

Figure 18. Model of slab element (plan of one side of equivalent slab reinforcement)

4.2. Individual response profiles

The complex connection behaviour was decomposed into the load–deformation characteristics of three important components such as bar deformations (top and bottom reinforcements), multi-spring elements (concrete) and tension slab element. Responses of each individual model components were examined in order to give a pre-validation for the general response of the subassembly. The hysteresis response of the force versus deformation for the three main components for simulating one of the test specimen JS is illustrated in Figure 19. The hysteresis response for the top and bottom mild steel are shown in Figures 19.a and 19.b, respectively. Figure 19.c shows the multi-spring responses for two selected springs within the ten springs, the first spring at the top face of the beam and the second one on the bottom face of the beam. Figure 19.d clearly demonstrated that the slab elements working range mainly within the tension zone. Figure 19.e shows the general response of the subassembly JS that was obtained using the proposed model for both cases, including and excluding the floor slab effect. This figure represents the combination of the individual responses due to the three components of connection.

5. Model verification and validation

To examine the ability of the proposed method in predicting the interior slab-beam-column subassemblies hysteretic loops, the model were initially used to evaluate the beam-column subassemblies with floor slab that were tested previously by Cheung et al [5], and Shin and LaFave [9]. Results obtained are drawn to the same scale in Figure 20, for the Cheung et al [5] experiments with good agreements in simulating both the beam (Figure 20.a) and column (Figure 20.b) responses.
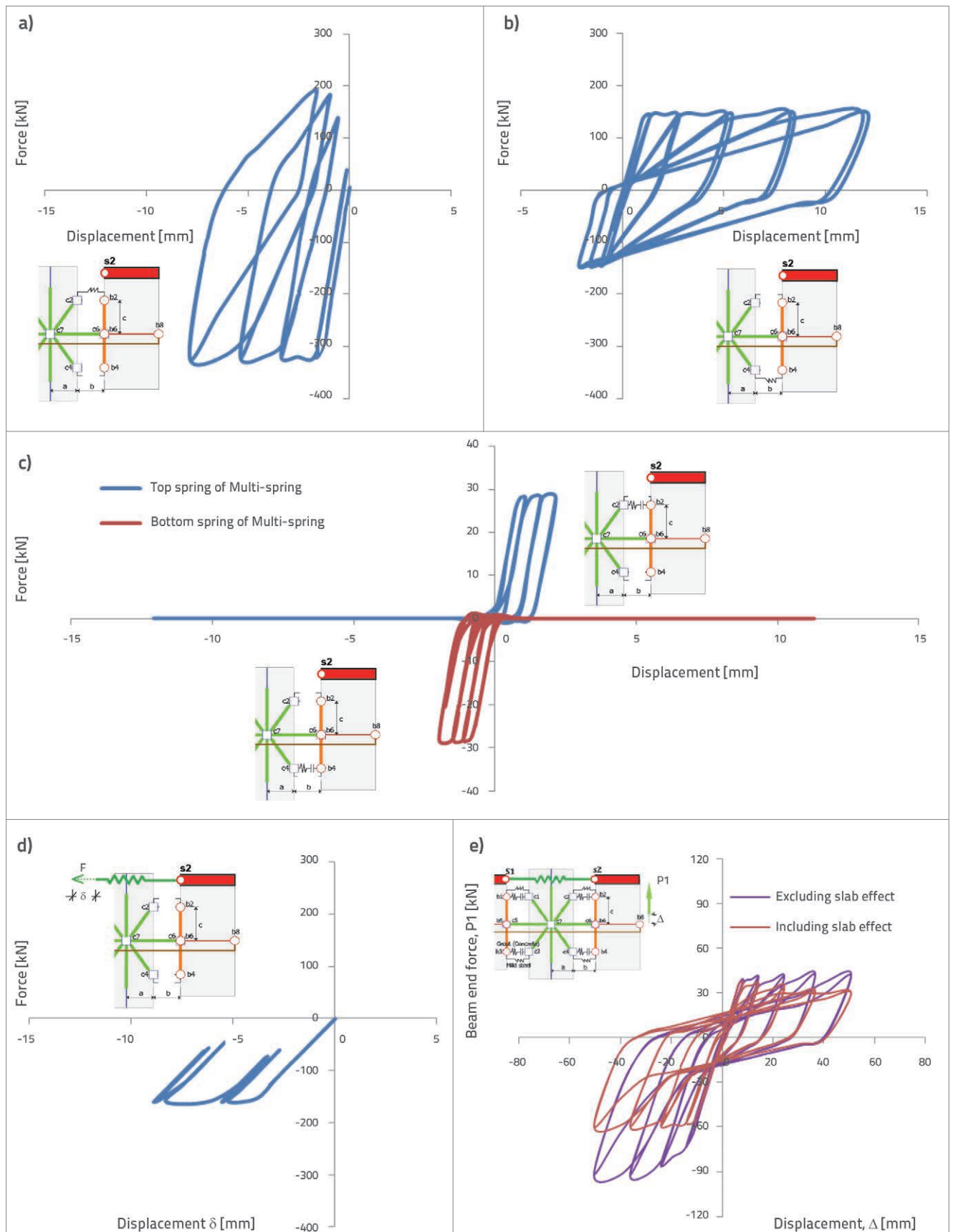
Figure 19. Individual response profile for modelling the specimen JS

Figure 21 shows the comparison of the current model results with the experiment results of Shin and LaFave [9] (specimen S3, without an eccentricity between main beam and column centrelines). The pinching effect (the middle part of each hysteretic loop was relatively narrow) did not capture; due to stiffness and strength degradation which were attributed to reinforcement bond slip losses through the joint region that occurred during the test. However, the general terms were the same.

Figure 21. Validation of model with tests performed by Shin and LaFave [9]

Consequently, results obtained from existing subassemblies test data were used also for the calibration of 2D joint models. Comparisons between experimental test results and numerical test results for both models with and without slab are shown in Figures 22 to 25. The current experimental and analytical comparisons lead to the following conclusions:

1. A satisfactory agreement between the numerical and experimental results is observed. The hysteretic curves (Figures 22 and 23) drawn to the same scale are the most significant results. Since the measured and computed values were similar during cyclic loading, the slab element effect at the subassemblies appeared to be significant.
2. The model can simulate with sufficient accuracy the loss of strength exhibited by some of the structural components. The pinching effects shown in the global behaviour are essentially caused by both yielding of the reinforcements and concrete cracking at the plastic hinge region.
3. The measured and computed cumulative energy dissipation, which contains aspects of both strength and deformation capacity, are relatively the same (Figure 24), confirming that the model works well.
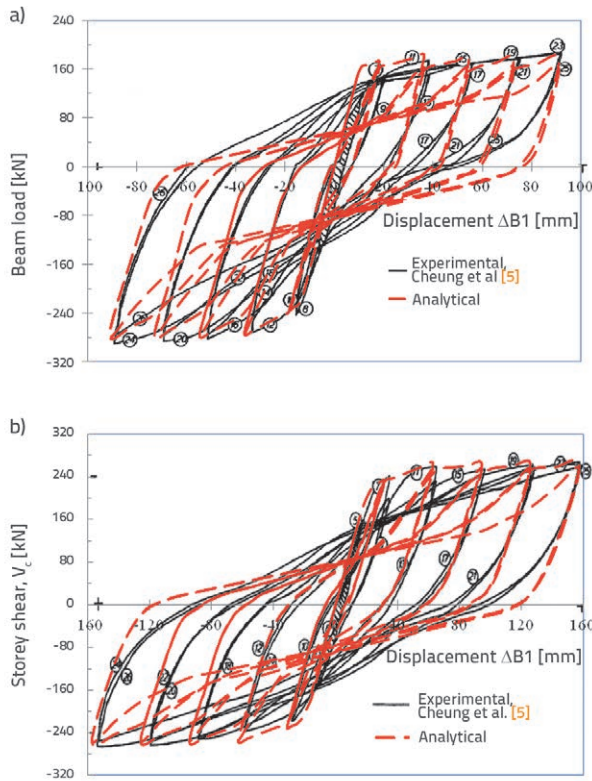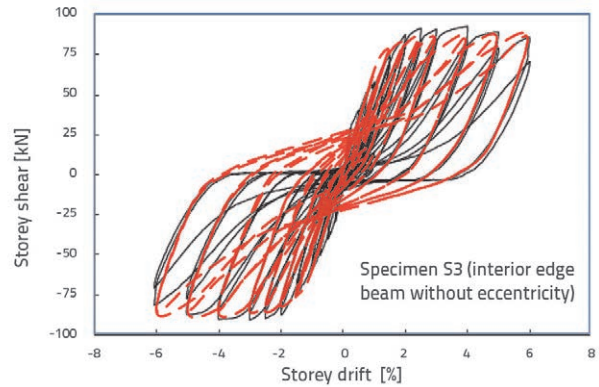

Figure 20. Validation of model with tests performed by Cheung et al [5]: a) Beam load vs tip beam displacement response; b) Storey shear vs column lateral displacement response
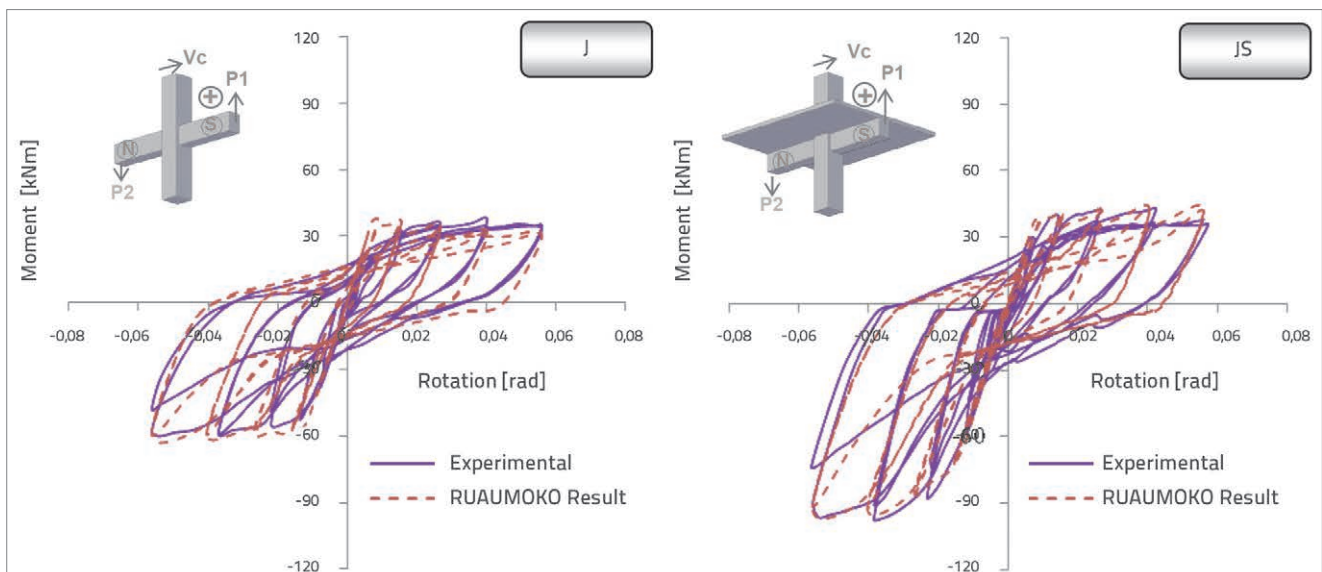

Figure 22. Simulation of hysteresis loops of beam flexural moment vs rotation
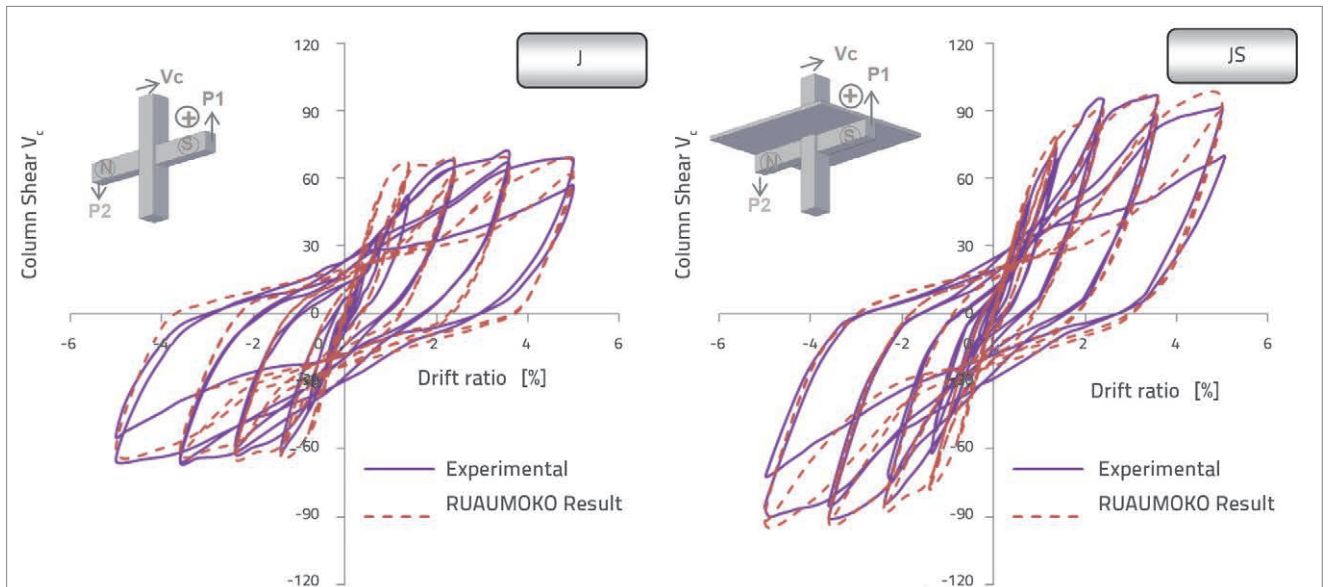
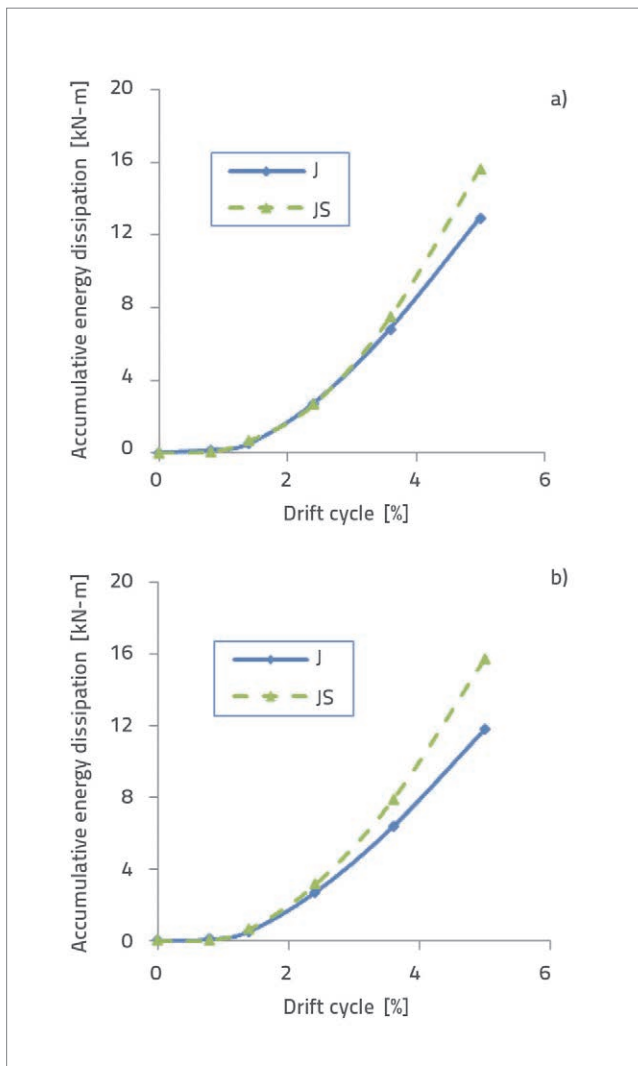Figure 23. Simulation of hysteresis loops of column shear vs drift ratio

Figure 24. Accumulative energy dissipation capacity; a) Experimental; b) Analytical
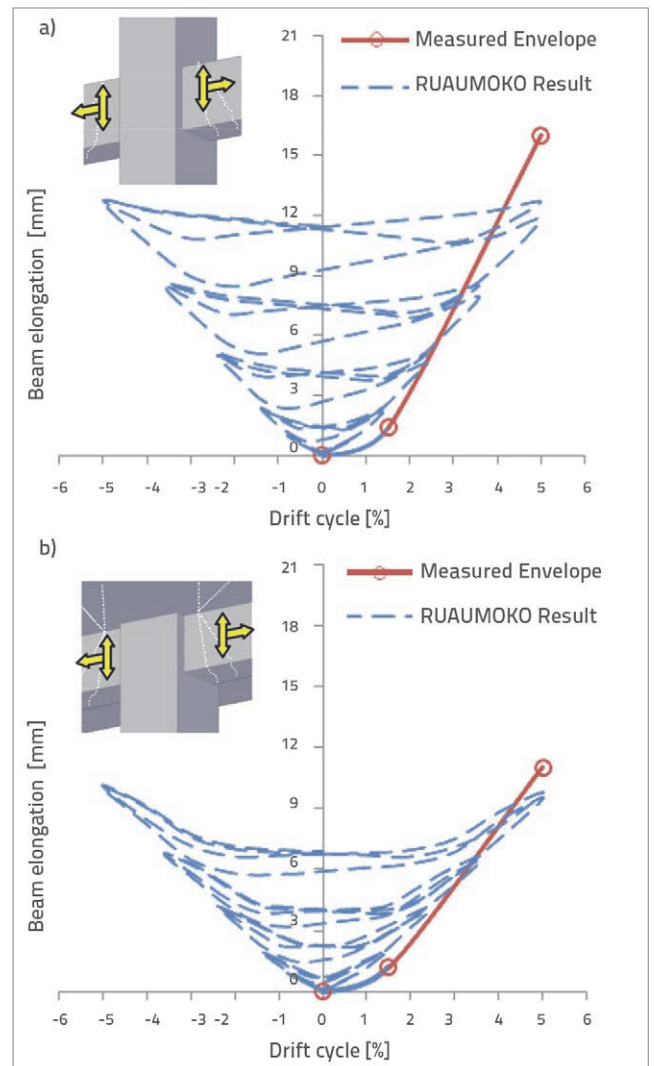

Figure 25. Beam elongation/relaxation vs drift ratio: a) Specimen J; b) Specimen JS

4. Both the models, including and excluding the slab effect can account for the influence of the member elongations with reasonable precision (Figure 25). Also the floor slab can significantly reduce this phenomenon, especially at a large deformation (drift ratio >1.5 %). This effect can be further observed in the analysis of the multi-connections frame; however, the elongation of the main beams is partially restrained by the exterior columns, which results in axial compression in the main beams.

6. Conclusions

In this research, the experimental and analytical study was conducted to investigate the behaviour of the interior beam-column joint subassemblies with and without slab. This study demonstrated that:

- Floor slabs can make a significant contribution to the flexural resistance of a structure, which is often ignored in the design for lateral loads. The experimental results showed a significant increase of the beam negative or hogging bending moment (67.1 %) and sagging strength (16.7 %). The increase in beam resistance due to the slab increases the column shear demands by 33 % on average in both directions of loading. The greater beam strength causes a greater column demand and this may be detrimental, as it can increase the possibility of soft storey mechanism or column shear failure, if it is not considered properly.

- The horizontal panel joint shear stress is increased due to the slab contribution, and is resisted within the joint by the inclined compression strut. However, the increased force along the strut may cause compression failure in the strut. Therefore, it is necessary to account for the enhancement of the beam strength due to the contribution from the slab, when considering the joint design. A large effective slab width would result in large shears in both the joint and in the beam that could result in premature shear failures.

- In reinforced concrete frames subjected to cyclic lateral loading, inelastic bending causes the beams to increase in length, called "beam elongation", and this beam elongation increases as the flexural inelastic deformation increases. Also the floor slab can significantly reduce this phenomenon, especially at large deformation levels (drift ratio >1.5 %).

- The result of this study indicated that the developed joint model predicts the test results with reasonable precision, and provides a simple way of accounting for the effects of slab and beam elongation, without a complicated nonlinear finite element modelling. However, to accurately evaluate the subassembly behavior, the cases with bond-slip loss within the joint should be considered.

REFERENCES

[1] Masi, A., Santarsiero, G., Nigro, D.: Cyclic tests on external RC beam–column joints: role of seismic design level and axial load value on the ultimate capacity, *Journal of Earthquake Engineering*, 17 (1), pp. 110-36, 2012.

[2] Paulay, T., Park, R., Priestley, M.: Reinforced concrete beam-column joints under seismic actions, ACI Structural Journal, 75 (11), pp. 585-593, 1978.

[3] Abdel-Fattah, B., Wight, K.: Study of moving beam plastic hinging zones for earthquake-resistant design of R/C buildings, *ACI Structural Journal*, 84 (1), pp. 31-39, 1987.

[4] Xilin, L., Tonny, U., Sen, L., Fangshu, L.: Seismic behavior of interior RC beam-column joints with additional bars under cyclic loading, *Earthquakes and Structures*, 3 (1), pp. 37-57, 2012.

[5] Cheung, P., Paulay, T., Park, R.: A reinforced concrete beam column joint of a prototype one-way frame with floor slab designed for earthquake resistance, *Research Report 87-6*, University of Canterbury, New Zealand, 1987.

[6] French, W., Moehle, P.: Effect of floor slab on behavior of slab-beam-column connections, design of beam-column joints for seismic resistance, *ACI Structural Journal*, SP-123, pp. 225-258, 1991.

[7] Alcocer, M., Jirsa, O.: Strength of reinforced concrete frame connections rehabilitated by jacketing, *ACI Structural Journal*, 90 (3), pp. 249-261, 1993.

[8] Aycardi, L., Mander, J., Reinhorn, A.: seismic resistance of reinforced concrete frame structures designed only for gravity loads: Experimental performance of subassemblage, *ACI Structural Journal,* 91 (5), pp. 552-563, 1995.

[9] Shin, M., LaFave, M.: Reinforced concrete edge beam–column–slab connections subjected to earthquake loading, *Magazine of Concrete Research,* 55 (6), pp. 273-291, 2004.

[10] ACI-ASCE Committee 352R: Recommendations for design of beam-column connections in monolithic reinforced concrete structures, *Reported by Joint ACI-ASCE Committee 352R*, Detroit, 2002.

[11] NZS 3101: New Zealand Standard-Model Building By-Laws Part, *New Zealand Standard Institute*; Wellington, New Zealand, 2006.

[12] CSA-A23.3: Design of Concrete Structures. *Canadian Standards Association,* Ontario, Canada; 2004.

[13] Durrani, J., Zerbe, E.: Seismic resistance of R/C exterior connections with floor slabs, *ASCE Journal of Structural Engineering,* 113 (8), pp. 1850-1864, 1987.

[14] Zerbe, E., Durrani, J.: Seismic response of connections in two-bay R/C frame subassemblies, *ASCE Journal of Structural Engineering,* 115 (11), pp. 2829-2844, 1989.

[15] Fenwick, R., Fong, A.: The behaviour of reinforced concrete beams under cyclic loading. *Research Report no.176,* Dept. of Civil Eng., Univ. of Auckland, New Zealand, 1979.

[16] Elwood, J., Pampanin, S., Kam, Y.: 22 February 2011 Christchurch earthquake and implications for the design of concrete structures, *in* Proc. *International Symp. on Eng. Lessons Learned from the 2011 Great East Japan Earthquake,* Tokyo, 2012.

[17] Youssef M, Ghobarah A. Modelling of RC beam–column joints and structural walls. *Journal of Earthquake Engineering*, 5 (1), pp. 93–111, 2001.

[18] Lowes, L., Altoontash, A.: Modeling reinforced-concrete beam-column joints subjected to cyclic loading, *ASCE Journal of Structural Engineering,* 129 (12), pp. 1686-1697, 2003.

[19] Mitra, N., Lowes, L.: Evaluation, calibration, and verification of a reinforced concrete beam-column joint model, *ASCE Journal of Structural Engineering,* 133 (1), pp. 105-120, 2007.

[20] Kim, J., LaFave, M.: Key influence parameters for the joint shear behavior of reinforced concrete (RC) beam–column connections, *Engineering Structures*, 29, pp. 2523-2539, 2007.

[21] Manfredi, G., Verderame, M., Lignola, P.: A F.E.M. model for the evaluation of the seismic behavior of internal joints in reinforced concrete frames. *In: 14th World conference on earthquake engineering,* Beijing, China, 2008.

[22] Sagbas, G., Vecchio, J., Christopoulos, C.: Computational modelling of the seismic performance of beam-column subassemblies, *Journal of Earthquake Engineering,* 15 (4), pp. 640-663, 2011.

[23] Fenwick, R., Davidson, B.: Elongation in ductile seismic resistant reinforced concrete frames, *in* Proc., *Tom Paulay Symp., Farmington Hills, Mich., American Concrete Institute,* SP 157 (7), pp. 143-170, 1995.

[24] Shahrooz, M., Pantazopoulou, J., Chern, P.: Modeling slab contribution in frame connections, *ASCE Journal of Structural Engineering,* 118 (9), pp. 2475-2494, 1992.

[25] MacRae, G., Umarani, C.: A concept for consideration of slab effects on building seismic performance, *in* Proc. *NZSEE New Zealand Society for Earthquake Engineering Conf.*, Christchurch, Paper no. 22, 2006.

[26] Lau, D.: Influence of precast prestressed flooring on the seismic performance of reinforced concrete perimeter frame buildings, *Report Number 653,* Dept. of Civil and Envi. Engg., Univ. of Auckland, New Zealand, 2007

[27] Peng, B.: Seismic performance assessment of reinforced concrete buildings with precast concrete floor systems, Ph.D. thesis, University of Canterbury, Christchurch, New Zealand, 2009.

[28] Unal, M., Burak, B.: Development and analytical verification of an inelastic reinforced concrete joint model, *Engineering Structures*, 52, pp. 284–294, 2013.

[29] Carr, A.: Ruaumoko 2D: User Manual, computer program library, Department of Civil Engineering, University of Canterbury, Christchurch, New Zealand, 2008.

[30] UBC, Handbook to the uniform building code: An Illustrative Commentary. Whittier, California: International Conference of Building Officials, 1997.

[31] ACI Committee 318: Building code requirements for reinforced concrete, American Concrete Institute, Detroit, 2002.

[32] ACI Committee 301: Specifications for Structural Concrete, American Concrete Institute, Detroit, 2002.

[33] ASTM C33: Standard specification for concrete aggregates, Annual Book of ASTM Standard, Philadelphia, 1989.

[34] ASTM C39: Practice standard test method for compressive strength of cylindrical concrete specimens, Annual Book of ASTM Standard, Philadelphia, 1989.

[35] Kim, J., Stanton, J., MacRae, G.: Effect of beam growth on reinforced concrete frames, *ASCE Journal of Structural Engineering*, 130 (9), pp. 1333-1342, 2004.

[36] Otani, S.: Hysteresis models of the reinforced concrete for earthquake response analysis, *Journal of Faculty of Engineering,* 36 (2), pp. 407-441, 1981.

[37] Priestley, M., Seible, F., Calvi, G.: *Seismic design and retrofit of bridges,* Wiley, New York, 1996.